Pyrolysis of wood and PVC mixtures: thermal behaviour and kinetic modelling

Augustina Ephraim, Victor Pozzobon, Damien Lebonnois, Carlos Peregrina, Patrick Sharrock, Ange Nzihou, Doan Pham Minh

Pyrolysis of wood and PVC mixtures: thermal behaviour and kinetic modelling

Augustina Ephraim [1] · Victor Pozzobon [2] · Damien Lebonnois [3] · Carlos Peregrina [3] · Patrick Sharrock [1] · Ange Nzihou [1] · Doan Pham Minh [4,1]

Abstract

Wood waste containing halogenated compounds such as polyvinyl chloride (PVC) is in abundant supply, although the pyrolysis of such waste feedstock for energy production may cause corrosion and environmental problems due to the release of HCl gas. Hence, there is a need to understand the pyrolysis behaviour of chlorine-contaminated wood in order to develop methods that minimise the impact of chloride species on pyrolysis equipment and product quality. In literature, few studies exist on the kinetic analysis of wood and PVC co-pyrolysis. The existing models assume a single-step reaction with an n-order reaction mechanism for the entire process, which may lead to large errors in the kinetic parameters estimated. Therefore, in this paper, we develop and validate a multi-step kinetic model that predicts the pyrolysis behaviour and reaction mechanism of poplar wood (PW) pellet with different contents of PVC (0, 1, 5, 10, 100 wt%). Using data from thermogravimetric analysis of the pellets at heating rates of 5, 10 and 20 °C/min, we determined the apparent kinetic parameters by combining Fraser-Suzuki deconvolution, isoconversional methods and master plot procedures. Our model fitted the experimental data well with a deviation of less than 4.5%. Our results show that the addition of 1 wt% PVC to PW decreases the activation energy of hemicellulose and cellulose pyrolysis in PW from 136.3 to 101.6 kJ/mol and from 216.7 to 108.2 kJ/mol, respectively. This demonstrates the importance of acid hydrolysis reactions between the cellulosic fibres of PW and HCl released from PVC dehydrochlorination. Furthermore, we found that a nucleation and growth mechanism best represents the rate-limiting interactions between PVC and PW, which we linked to the formation of metal chloride crystals from acid-base reactions between HCl and PW minerals. Our kinetic model is an improvement of current models for the co-pyrolysis of wood and PVC, and can be readily used in a reactor-scale model of a pyrolyser or gasifier due to its relative simplicity.

Keywords Waste · Co-pyrolysis · Wood · Polyvinyl chloride · Kinetic modelling · Reaction mechanism

1 Introduction

Wood waste is an attractive feedstock for renewable energy production *via* pyrolysis/gasification, mainly due to its abundant supply, low recycling rate and good fuel properties [1]. Syngas generated from pyrolysis/gasification as the main product can be purified and upgraded into various valuable final products such as chemicals, biofuels and biomass-derived hydrogen. As an example, Scheme 1 illustrates the main steps of biomass-derived hydrogen production from wood waste [2]. Purified syngas passes through water-gas-shift (WGS) reactors under appropriate conditions to convert CO and steam into H_2 and CO_2 [3]. The mixture from WGS reactors' outlet is rich in H_2. Pure biomass-derived hydrogen can be separated from this mixture by an operation like pressure-swing-adsorption (PSA) [2, 4].

✉ Doan Pham Minh
phamminhdoan@duytan.edu.vn; doan.phamminh@mines-albi.fr

[1] Université de Toulouse, IMT Mines Albi, UMR CNRS 5302, Centre RAPSODEE, Campus Jarlard, F-81013, cedex 09 Albi, France

[2] LGPM, Centrale Supelec, Université Paris-Saclay, SFR Condorcet FR CNRS 3417, Centre Européen de Biotechnologie et de Bioéconomie (CEBB), 3 rue des Rouges Terres, 51110 Pomacle, France

[3] SUEZ, 38, rue du Président Wilson, 78230 Le Pecq, France

[4] Institute of Research and Development, Duy Tan University, Da Nang 550000, Vietnam

Scheme 1 Main steps to produce biomass-derived hydrogen from wood waste

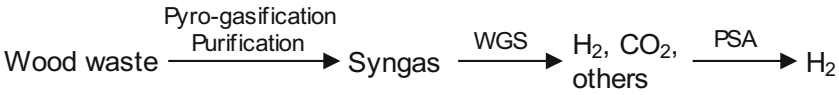

However, chemically treated wood waste with halogenated compounds such as polyvinyl chloride (PVC) may have significant chlorine content. In pyrolysers, chlorine in such waste readily vaporises at moderate temperatures (> 200 °C) to mainly form hydrogen chloride gas (HCl), which causes corrosion, environmental damages and health-related problems. Dioxins could be also formed on solid surfaces at 200–400 °C, and their formation is enhanced by the presence of chlorine compounds such as PVC [5]. Consequently, it is important to understand and predict the thermal decomposition behaviour of wood waste containing PVC in order to better control the hazardous impact of chloride species on pyrolysis systems and product quality.

In the last decade, several authors have studied the co-pyrolysis of PVC and different biomass/wastes using thermogravimetric analysis (TGA), and all have observed strong interactions in terms of lower pyrolysis temperatures of biomass/waste in the presence of PVC [6–13]. However, very few kinetic analyses of these interactions have been found in literature. A complete kinetic study of such a co-pyrolysis process requires the determination of the kinetic triplet: namely, the activation energy E, the pre-exponential factor A, and the kinetic model f(α) [14].

Abdoulkas et al. [15] have studied the reactivity of co-pyrolysed olive residue and PVC using the isoconversional Friedman method to determine E_α. The entire pyrolysis process was considered a single-step reaction which led to a significant variation of E_α with conversion α. According to the Kinetics Committee of the International Confederation for Thermal Analysis and Calorimetry (ICTAC) [16], a significant variation of E_α with α indicates that the pyrolysis process is kinetically complex and thus, it is inappropriate to use a single-step rate equation to describe the kinetics of this process throughout the whole range of conversions and temperatures.

More recent kinetic analyses by Han et al. [8] and Çepelioğullara et al. [9] also suffer from this limitation of a single-step co-pyrolysis model. Furthermore, these models assume that the co-pyrolysis mechanism is first-order ($f(\alpha) = 1 - \alpha$) without reporting arguments that support this assumption. Recent works have proven that the pyrolysis of polymers does not necessarily take place through first- or n-order kinetics and that other mechanisms such as diffusion or random scission can control the decomposition reaction [17–19]. In such cases, this often yields higher A and E_α values than the true values and particularly give A values that are too large to be physically reasonable [17]. Other approaches such as distributed activation energy model (DAEM) are weak to interpret the reaction mechanism [20]. Facing such a problem, it is necessary to consider using other kinetic models ($f(\alpha)$) to fit the experimental data.

The objective of this work, therefore, is to develop a multi-step apparent kinetic model for the co-pyrolysis of PVC and poplar wood (PW) pellets and to identify the mechanisms that govern their interactions. This work combines the use of Fraser-Suzuki deconvolution and isoconversional Kissinger-Akahira-Sunose (KAS) methods to determine the apparent E_α for each pseudo-component in the PVC/PW mixture, as well as the master-plot procedure to determine the reaction mechanisms $f(\alpha)$, and eventually A. Deconvolution allows identifying the peak of each species from a global signal, while isoconversional method is related to the investigation of a transformation at the same conversion, by changing a parameter (e.g. heating rate in this work).

2 Thermal analysis method

2.1 Preparation of poplar wood–PVC pellets

The PW sample used in this study was obtained from Special Diets Services (SDS). It was first dried at 105 °C for 24 h and then ground into fine powder with a particle size < 100 μm. The PVC samples were provided by Analytic Lab with a particle size of approximately 130 μm. To prepare 0, 1, 5, 10 and 100 wt% PVC/PW pellets, the samples were first weighed and then mixed using pestle and mortar. The mixture was then pressed manually at 10 bar to produce 500 mg pellets of < 3 mm thickness. Table 1 shows the proximate and ultimate analysis of the PW and PVC samples as well as their major inorganic element composition.

2.2 Thermogravimetric apparatus and procedure

Thermogravimetric analysis of the samples was performed under atmospheric pressure using a TGA/DTA analyser (STA 409 PC, Netzsch). Samples of 500 mg were placed in platinum crucibles and heated from 30 to 800 °C at rates of 5, 10 and 20 °C/min under nitrogen atmosphere (100 mL/min). Each heating rate run was repeated twice and the mass loss data were found to be repeatable (error < 1%).

Table 1 Proximate, ultimate and major inorganic ash element analysis of poplar wood (PW) and PVC

Sample	PW	PVC
Proximate analysis (wt%, ar)		
Moisture	8.4	0.0
Ash	2.0	0.0
Volatiles	85.1	95.8
Fixed carbon	4.5	4.2
Ultimate analysis (wt%, daf)		
C	49.9	38.7
H	6.4	4.8
O	42.7	0.0
N	1.0	0.0
S	0.00	0.0
Cl	0.01	56.5
Major inorganic ash elements (ppm, ar)		
Ca	3981	0.0
K	655	0.0
Na	382	0.0
Mg	384	0.0
P	340	0.0

3 Thermal analysis results

3.1 Pyrolysis of pure poplar wood and PVC

Figure 1a shows the TG/DTG curves for the pyrolysis of 100 wt% PW at heating rates of 5, 10 and 20 °C/min. These curves show the typical behaviour of wood pyrolysis: a shoulder appears at 190–290 °C which corresponds to hemicellulose decomposition; a sharp peak is observed at 290–360 °C owing to cellulose decomposition; and the broad, low magnitude tailing at 360–500 °C can be linked to lignin degradation [21].

Concerning the pyrolysis of PVC, three main degradation steps could be observed in Fig. 1b. The first step, which occurs at 200–350 °C, is the dehydrochlorination of PVC to form HCl and polyene. In the second step (300–350 °C), the polyene molecules produced subsequently undergo condensation and de-alkylation reactions to form benzene and aromatic compounds, e.g. C_6H_6, $C_{10}H_{10}$, C_8H_9Cl, and $C_{18}H_{15}Cl$ [22, 23]. Finally, above 350 °C, cyclisation and cross-linking of polyene molecules occur to form polyaromatic hydrocarbons (PAH) and char residues [22, 23].

The effect of the heating rate can be seen in Fig. 1 for both PW and PVC. As the heating rate increases, the TG/DTG curves shift towards higher temperatures. This phenomenon has also been observed in other literature works involving TGA [24, 25] and is due to heat transfer limitations resulting from the temperature difference between the sample and the furnace. In such instances, the thermal lag is more pronounced at higher heating rates, which in turn slows down the decomposition rate. Even though this phenomenon can be observed, it is thought to have only a minor impact on our model results (maximum deviation of 4.5%, cf. Table 5 and Table 6).

3.2 Co-pyrolysis of PVC and poplar wood

Figure 2 presents the TG/DTG curves for the pyrolysis of 1, 5 and 10 wt% PVC/PW pellet samples at heating rates of 5, 10 and 20 °C/min. By comparing these TG/DTG curves to those of 100 wt% PW and PVC in Fig. 1, the following observations can be made:

- The presence of PVC shifts the DTG peaks of hemicellulose and cellulose decomposition in wood towards lower temperatures. For example, at a heating rate of 5 °C/min, cellulose in pure wood degrades with a DTG peak at approximately 332 °C. However, in the presence of 1, 5 and 10 wt% PVC, this temperature is lowered by 2, 55, and 60 °C, respectively. These lower temperatures thus approach the DTG peak temperature of PVC dehydrochlorination (266 °C).
- With respect to pure wood, the addition of PVC significantly increases the height of the DTG peaks at 200–300

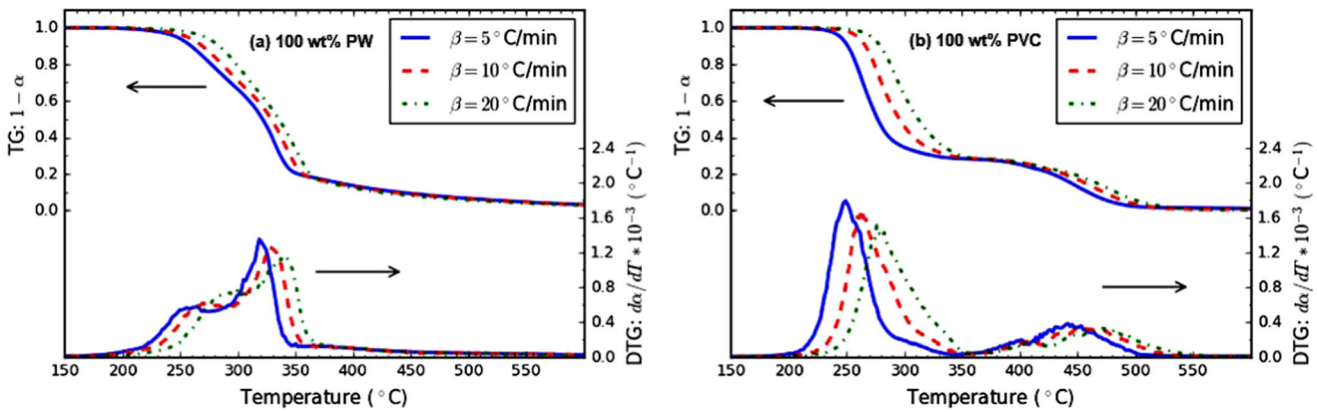

Fig. 1 TG and DTG curves of **a** pure poplar wood (PW) and **b** and PVC pellets at heating rates of 5, 10 and 20 °C/min

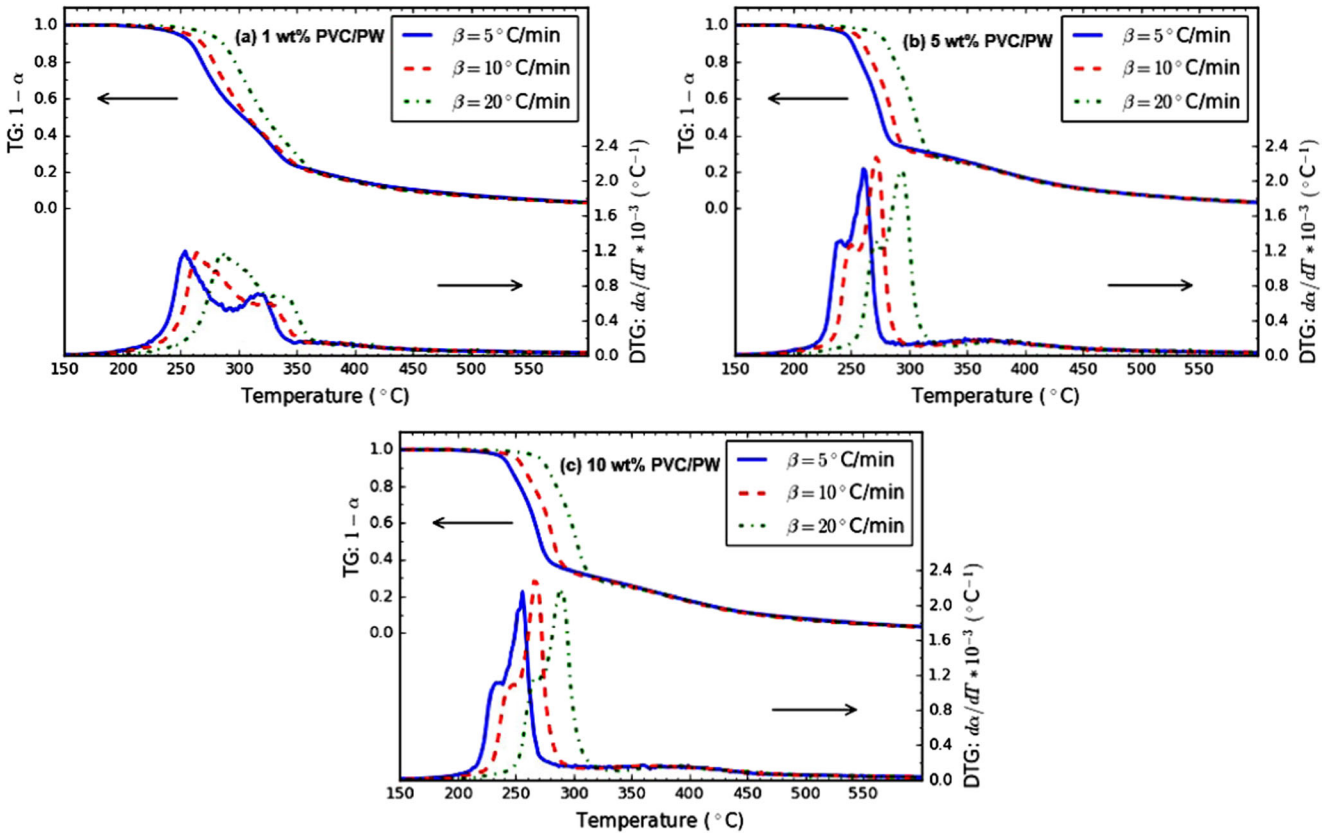

Fig. 2 TG and DTG curves of pellets of **a** 1 wt%, **b** 5 wt%, and **c** 10 wt% PVC/poplar wood (PW) pellets at heating rates of 5, 10 and 20 °C/min

°C, which relates to cellulosic fibre degradation. For instance, at a heating rate of 5 °C/min, the corresponding DTG peak heights for 1, 5 and 10 wt% PVC increase by a factor of 2.10, 3.77 and 3.80, respectively, compared with pure wood pyrolysis. Furthermore, in the case of 5 wt% and 10 wt% PVC/PW samples, the DTG peak heights increase by a factor of 1.19 and 1.20 respectively compared with pure PVC pyrolysis.

- At temperatures between 350 and 500 °C, the conversion of 10 wt% PVC/PW is only 4% more than that of 100 wt% PW. Hence, lignin in PW can be considered largely unaffected by the cyclisation/cross-linking step in PVC pyrolysis.

The above observations are indicative of the strong interaction between the cellulosic components of PW and HCl released during PVC dehydrochlorination.

Another point worth noting is the very small difference in the pyrolysis behaviour of 5 and 10 wt% PVC/PW.

This implies that most, if not all, of the cellulosic fibres in wood react with the chlorinated species products during co-pyrolysis with PVC concentrations as low as 5 wt%. HCl released from dehydrochlorination of PVC has been considered a catalyst of cellulosic fibre degradation [6, 8]. However, this is not the case for 1 wt% PVC, because a second DTG peak corresponding to cellulose decomposition appears at roughly 330 °C (Fig. 2) and thus, not all the cellulose decomposes during the dehydrochlorination step. Matsuzawa et al. [13] also observed a second DTG peak at approximately 300 °C for a mixture of 2 wt% PVC and a pure cellulose polymer.

4 Kinetic modelling approach

4.1 Model assumptions and reaction scheme

To describe the TG/DTG curves of pure poplar wood, a three-component devolatilisation mechanism is proposed for the volatile fractions of its pseudo-components, hemicellulose (H), cellulose (C) and lignin (L). These pseudo-components decompose independently of each other as shown by Eq. 1 to Eq. 3.

$$H \xrightarrow{k_1,\ PW} V_H \tag{1}$$

$$C \xrightarrow{k_2,\ PW} V_C \tag{2}$$

$$L \xrightarrow{k_3,\ PW} V_L \tag{3}$$

where k refers to the reaction rate constant and V is the gas released from each devolatilisation reaction. Some mineral matter in wood may also volatilise during pyrolysis, but they generally make up a small mass fraction of wood and are therefore not considered in this reaction scheme. A three-component mechanism is also proposed for PVC, involving the pseudo-components, HCl and polyene (P), as expressed by Eq. 4 to Eq. 6:

$$HCl \xrightarrow{k_1,\ PVC} V_{HCl} \tag{4}$$

$$P1 \xrightarrow{k_2,\ PVC} V_{P1} \tag{5}$$

$$P2 \xrightarrow{k_3,\ PVC} V_{P2} \tag{6}$$

where $P1$ refers to the polyene molecules that volatilise as a result of condensation and de-alkylation reactions, and $P2$ are the polyene molecules that degrade by cyclisation and cross-linking reactions.

A global reaction scheme is also proposed for the interactions between the pseudo-components of PW and PVC during co-pyrolysis (Eq. 7 to Eq. 12). Here, only the dehydrochlorination phase in PVC pyrolysis is considered, which, for convenience sake, is represented by the volatilisation of HCl pseudo-component. Hemicellulose and cellulose in PW decompose to release volatiles via two parallel reactions: thermal degradation and acid hydrolysis. Finally, lignin only undergoes thermal degradation because it mainly decomposes after HCl release.

$$H \xrightarrow{k_1,\ PVC/PW} V_H \tag{7}$$

$$C \xrightarrow{k_2,\ PVC/PW} V_C \tag{8}$$

$$L \xrightarrow{k_3,\ PVC/PW} V_L \tag{9}$$

$$HCl \xrightarrow{k_4,\ PVC/PW} V_{HCl} \tag{10}$$

$$H\text{–}HCl \xrightarrow{k_5,\ PVC/PW} V_{H\text{–}HCl} \tag{11}$$

$$C\text{–}HCl \xrightarrow{k_6,\ PVC/PW} V_{C\text{–}HCl} \tag{12}$$

With regard to modelling 1 wt% PVC/PW pyrolysis, all six reactions in Eq. 7 to Eq. 12 are assumed to take place, thus leading to a six-pseudo-component devolatilisation model. However, for 5 and 10 wt% PVC/PW, a four-pseudo-component model is considered because the hydrolysis rate of hemicellulose and cellulose is expected to be much faster than the thermal degradation rate in the presence of high HCl concentrations. Thus, in the case of high PVC concentrations (5 or 10 wt%), reactions 1 and 2 (or 7 and 8) are assumed to be negligible.

4.2 TGA kinetics

The expression for the rate of solid-state reactions has the following form:

$$\frac{d(\alpha)}{dt} = k(T)f(\alpha) \tag{13}$$

The conversion, α, is the fraction of the initial sample decomposed:

$$\alpha = \frac{m_o - m}{m_o - m_\infty} \tag{14}$$

where m_o and m_∞ are the initial and final mass of the sample, and m is the mass at a given time t of the analysis. According to the Arrhenius equation, the temperature dependence on the rate constant, k, is given by:

$$k = Aexp\left(\frac{-E}{RT}\right) \tag{15}$$

where A is the pre-exponential factor (min^{-1}), E is the activation energy (kJ/mol), R is the gas constant (8.314 J/K/mol) and T is the absolute temperature (K). Combining Eq. 13 and Eq. 15 gives the fundamental expression (Eq. 16) to determine the kinetic parameters that satisfactorily describe the TGA results:

$$\frac{d\alpha}{dt} = Aexp\left(\frac{-E}{RT}\right)f(\alpha) \tag{16}$$

For non-isothermal TGA experiments at linear heating rate, $\beta = dT/dt$; thus, Eq. 16 can be expanded to:

$$\frac{d\alpha}{dT} = \left(\frac{A}{\beta}\right)exp\left(\frac{-E}{RT}\right)f(\alpha) \tag{17}$$

4.3 Fraser-Suzuki deconvolution

Deconvolution of the DTG peaks can be performed using a Fraser-Suzuki function (FSF) [25].

$$\left.\frac{d\alpha}{dT}\right|_i = H_{p,i}exp\left\{-\frac{ln2}{A_{s,i}^2}ln\left[1 + 2A_{s,i}\frac{T - T_{p,i}}{W_{hf,i}}\right]^2\right\} \tag{18}$$

The FSF parameters, H_p, A_s, T_p, and W_{hf}, represent height (K^{-1}), asymmetry (dimensionless), peak temperature (K) and half-width (K) of the $d\alpha/dT$ versus T profile for the ith pseudo-component respectively. Hence, for wood and PVC pyrolysis, the deconvolution of the $d\alpha/dT$ versus T profile gives:

$$\frac{d\alpha}{dT} = \sum_{i=1}^{N_c} c_i H_{p,i}exp\left\{-\frac{ln2}{A_{s,i}^2}ln\left[1 + 2A_{s,i}\frac{T - T_{p,i}}{W_{hf,i}}\right]^2\right\} \tag{19}$$

where c_i and N_c are the mass fraction of the ith pseudo-component and the total number of pseudo-components of each sample respectively. To estimate the unknown parameters, c_i, H_p, A_s, T_p, and W_{hf} were initially guessed and then

adjusted until the deviation between the calculated and experimental values for $d\alpha/dT$ was minimised. The deviation $Dev(\%)$ was calculated using nonlinear least squares [25]:

$$Dev(\%) = \frac{\sqrt{\left(\sum_{j=1}^{N_d}\left[\left(\frac{d\alpha}{dT}\right)_{j,e} - \left(\frac{d\alpha}{dT}\right)_{j,c}\right]^2\right)/N_d}}{h} \quad (20)$$

where j denotes the jth experimental point and N_d is the total number of data points. $(d\alpha/dT)_{j,\,c}$ and $(d\alpha/dT)_{j,\,e}$ are the calculated and experimental DTG data, and h is the maximum value of $d\alpha/dT$. Note that the calculated DTG data is the sum of all the deconvoluted peaks.

Next, the separated $d\alpha/dT$ curves were each integrated using the middle Riemann sum method [26] to obtain α values for each component i:

$$\alpha_i = \sum_{j=1}^{N_d} \frac{1}{2}\left[\left(\frac{d\alpha}{dT}\right)_j + \left(\frac{d\alpha}{dT}\right)_{j-1}\right](T_j - T_{j-1}) \quad (21)$$

4.4 Activation energy determination using KAS method

The integral rearrangement of Eq. 16 gives:

$$g(\alpha) = \int_0^\alpha \frac{1}{f(\alpha)}d\alpha = \frac{A}{\beta}\int_{T_o}^{T} exp\left(\frac{-E}{RT}\right)dT \quad (22)$$

where $g(\alpha)$ is the integral form of $f(\alpha)$. $f(\alpha)$ is a function for the algebraic expression that represents the mechanism of the solid-degradation process. The most common forms of f(α) and corresponding g(α) are listed in Table 2.

Kissinger-Akahira-Sunose (KAS) method [16] linearises Eq. 22 to obtain the following expression:

$$ln\left(\frac{\beta}{T_\alpha^2}\right) = ln\left(\frac{A_\alpha R}{E_\alpha g(\alpha)}\right) - \frac{-E}{RT_\alpha} \quad (23)$$

The apparent activation energy can be obtained from the plot of $ln(\beta/T_\alpha^2)$ versus $1000/T_\alpha$ for a given value of conversion, α, where the slope of the straight line is equal to $-E_\alpha/R$. Once the most suitable $f(\alpha)$ is known, the pre-exponential factor, A_α, can be calculated from the intercept.

4.5 Master plots

The most suitable reaction mechanism of pyrolysis, $f(\alpha)$, can be determined using the generalised master plots method [15].

$$\lambda(\alpha) = \frac{f(\alpha)}{f(\alpha)_{0.5}} = \frac{(d\alpha/dt)_\alpha}{(d\alpha/dt)_{0.5}}\frac{exp[E_o/RT_\alpha]}{exp[E_o/RT_{0.5}]} \quad (24)$$

where $(d\alpha/dt)_{0.5}$ and $T_{0.5}$ are the conversion rate and temperature corresponding to $\alpha = 0.5$, respectively. E_o is the average activation energy determined using the KAS method. The suitable pyrolysis reaction mechanism is obtained when the model $\lambda(\alpha)$ best matches the experimental $\lambda(\alpha)$.

Table 2 The most common reaction mechanism functions used in kinetic analysis of solid-state reactions [25, 27, 28]

Model		$f(\alpha) = (1/k)(d\alpha/dt)$	$g(\alpha) = kt$
Power law	Pn Power law	$n(\alpha)^{(n-1)/n}$	$\alpha^{1/n}$
Nucleation and growth	A2 Avrami-Erofeev	$2(1-\alpha)[-ln(1-\alpha)]^{1/2}$	$[-ln(1-\alpha)]^{1/2}$
	A3 Avrami-Erofeev	$3(1-\alpha)[-ln(1-\alpha)]^{2/3}$	$[-ln(1-\alpha)]^{1/3}$
	A4 Avrami-Erofeev	$4(1-\alpha)[-ln(1-\alpha)]^{3/4}$	$[-ln(1-\alpha)]^{1/4}$
	B1 Prout-Trompkins	$\alpha(1-\alpha)$	$ln(\alpha/(1-\alpha))$
Geometrical models	R2 contracting area	$2(1-\alpha)^{1/2}$	$1-(1-\alpha)^{1/2}$
	R3 contracting volume	$3(1-\alpha)^{2/3}$	$1-(1-\alpha)^{1/3}$
Diffusion models	D1 one-dimensional	$1/2\alpha$	α^2
	D2 two-dimensional	$[-ln(1-\alpha)]^{-1}$	$(1-\alpha)ln(1-\alpha)+\alpha$
	D3 three-dimensional	$3/2(1-\alpha)^{2/3}[1-(1-\alpha)^{1/3}]$	$1-((1-\alpha)^{1/3})^2$
	D4 Ginstling-Brounshein	$3/2[(1-\alpha)^{-1/3}-1]^{-1}$	$1-(2\alpha/3)-(1-\alpha)^{2/3}$
Order-based models	F0 zero order	1	α
	F1 first order	$1-\alpha$	$-ln(1-\alpha)$
	F2 second order	$(1-\alpha)^2$	$[1/(1-\alpha)]-1$
	F3 third order	$(1-\alpha)^3$	$[1/(1-\alpha)^2]-1$
Random scission model	L2	$2(\alpha^{1/2}-\alpha)$	–

$g(\alpha)$ is the integral form of $f(\alpha)$

5 Kinetic modelling results

5.1 Fraser-Suzuki deconvolution results

The Fraser-Suzuki deconvolution parameters for pure PW and PVC pyrolysis at 5, 10 and 20 °C/min are listed in Table 3, and those for 1, 5 and 10 wt% PVC/PW mixtures are shown in Table 4. The deconvolution models fit the experimental data satisfactorily with low deviation values (< 4%) which were calculated using Eq. 20. Figure 3 gives an example of the deconvolution curves of the samples at a heating rate of 5 °C/min.

5.2 Isoconversional activation energy results

Following the separation of the DTG peaks (Fig. 3), the middle Riemann sum integral method (Eq. 21) was employed to obtain the conversion values α, with respect to temperature for each pseudo-component at all three heating rates (5, 10, 20 °C/min). Next, the isoconversional activation energy of each pseudo-species decomposition was evaluated at a given α from the slope of the KAS plot in Eq. 23, i.e. $ln\left(\beta/T_\alpha^2\right)$ versus $1/T_\alpha$ plot. As an example, Fig. 4 presents the KAS plots for all six components of 1 wt% PVC/PW in the conversion range of 0.10 to 0.90. Correlation coefficient values (R^2) ranging between 0.9900 and 1 were obtained from linear regression analysis of these plots, which indicates that the activation energies calculated are relatively accurate.

Figure 5 displays the evolution of activation energy (E_α) with conversion α, calculated for the pseudo-components of pure PW and PVC as well as their mixtures. According to the ICTAC Kinetics Committee [16], E_α values are considered to vary significantly with α if the difference between the maximum and minimum values of E_α is above 20–30% of the average E_α. From Fig. 5, it can be observed that E_α values for the co-pyrolysis pseudo-species (H-HCl and C-HCl) and those of pure PVC (HCl, P1 and P2), are roughly constant with variations of < 16% over the entire conversion range. Thus, it is likely that the decomposition of each of these pseudo-components is dominated by a single reaction mechanism and can therefore be adequately described by a single-step model [16]. However, higher E_α variations with α can be observed for hemicellulose (29%), cellulose (22%) and lignin

Table 3 Fraser-Suzuki deconvolution results for pure PW and PVC at 5, 10 and 20 °C/min

Component		100 wt% PM			100 wt% PVC		
		5 °C/min	10 °C/min	20 °C/min	5 °C/min	10 °C/min	20 °C/min
H	H_p	0.51	0.53	0.58	-	-	-
	T_p	275	287.75	300.5	-	-	-
	W_{hf}	53	53	51	-	-	-
	A_s	− 0.06	− 0.10	− 0.10	-	-	-
	c_i	0.33	0.34	0.35	-	-	-
C	H_p	1.30	1.20	1.1	-	-	-
	T_p	332	341.75	351.9	-	-	-
	W_{hf}	25	27	29	-	-	-
	A_s	− 0.40	− 0.40	− 0.40	-	-	-
	c_i	0.42	0.41	0.41	-	-	-
L	H_p	0.11	0.105	0.1	-	-	-
	T_p	371.5	380.5	391	-	-	-
	W_{hf}	185	190	195	-	-	-
	A_s	0.20	0.31	0.45	-	-	-
	c_i	0.25	0.25	0.24	-	-	-
HCl	H_p	-	-	-	1.60	1.55	1.4
	T_p	-	-	-	266	279.5	293
	W_{hf}	-	-	-	33	33	33
	A_s	-	-	-	0.00	0	0
	c_i	-	-	-	0.55	0.57	0.56
P1	H_p	-	-	-	0.3	0.3	0.33
	T_p	-	-	-	290	306	322
	W_{hf}	-	-	-	50	50	50
	A_s	-	-	-	0.2	0.2	0.2
	c_i	-	-	-	0.16	0.16	0.18
P2	H_p	-	-	-	0.35	0.3	0.28
	T_p	-	-	-	447	460	473
	W_{hf}	-	-	-	77.5	85	85
	A_s	-	-	-	0	0	0
	c_i	-	-	-	0.29	0.28	0.26
Dev (%)		1.99	1.63	2.23	1.48	1.99	2.85

Table 4 Fraser-Suzuki deconvolution results for of 1, 5 and 10 wt% PW/PVC pellets at 5, 10 and 20 °C/min

Component		1 wt% PVC/PW			5 wt% PVC/PW			10 wt% PVC/PW		
		5 °C/min	10 °C/min	20 °C/min	5 °C/min	10 °C/min	20 °C/min	5 °C/min	10 °C/min	20 °C/min
H	H_p	0.16	0.18	0.2	-	-	-	-	-	-
	T_p	275	287.75	300.5	-	-	-	-	-	-
	W_{hf}	53	53	51	-	-	-	-	-	-
	A_s	− 0.06	− 0.1	− 0.1	-	-	-	-	-	-
	c_i	0.11	0.12	0.13	-	-	-	-	-	-
C	H_p	0.72	0.63	0.67	-	-	-	-	-	-
	T_p	332	341.75	351.5	-	-	-	-	-	-
	W_{hf}	25	27	29	-	-	-	-	-	-
	A_s	− 0.4	− 0.4	− 0.4	-	-	-	-	-	-
	c_i	0.25	0.23	0.26	-	-	-	-	-	-
L	H_p	0.11	0.1	0.1	0.16	0.14	0.14	0.15	0.14	0.14
	T_p	371.5	380.5	391	371.5	380.5	391	371.5	380.5	391
	W_{hf}	185	190	195	185	190	195	185	190	195
	A_s	0.2	0.31	0.45	0.2	0.31	0.45	0.2	0.31	0.45
	c_i	0.27	0.25	0.24	0.35	0.32	0.35	0.34	0.33	0.33
HCl	H_p	0.0128	0.0134	0.014	0.0735	0.073	0.0724	0.137	0.136	0.143
	T_p	266	279.5	293	266	279.5	293	266	279.5	293
	W_{hf}	33	33	33	33	33	33	33	33	33
	A_s	0	0	0	0	0	0	0	0	0
	c_i	0.0055	0.0056	0.0056	0.0282	0.0289	0.0283	0.0552	0.0555	0.0559
H-HCl	H_p	0.9	0.93	0.93	1.1	1.1	1.1	0.95	0.95	1
	T_p	267	280	298.5	255	268.5	286	250	264	282
	W_{hf}	20	20	20	20	20	20	20	20	20
	A_s	0	0	0	0	0	0	0	0	0
	c_i	0.23	0.23	0.22	0.25	0.26	0.26	0.22	0.22	0.24
C-HCl	H_p	0.59	0.72	0.7	2	2	2	1.95	2	2
	T_p	284	301	318	275	288	307	270	283	303
	W_{hf}	16	16	16	16	16	16	16	16	16
	A_s	0	0	0	0	0	0	0	0	0
	c_i	0.13	0.15	0.14	0.38	0.39	0.38	0.39	0.39	0.38
Dev (%)		3.9	3.9	3.1	1.8	2.3	1.4	1.7	1.8	1.2

(35%) in pure PW as they are more kinetically complex. Because the pyrolysis of lignin takes place over several stages, and its decomposition occurs over a wide temperature range, it would therefore be more appropriate to apply multi-step kinetics to treat this process. However, this lies beyond the scope of the current work and, thus, some loss of accuracy in lignin decomposition kinetics will be tolerated in order to favour reliable kinetic predictions of the interactions between the cellulosic pseudo-components of PW and HCl from PVC.

The average apparent activation energies obtained for cellulose, hemicellulose and lignin in PW are 216, 136 and 112 kJ/mol respectively. These results fall within the range of activation energies in literature for biomass pseudo-components, as summarised in a recent review by Anca-Couce [29]. For PVC, the pseudo-species, HCl, P1 and P2, have an average E_α of 120, 112, and 226 kJ/mol. Similar to biomass pyrolysis, literature values for the activation energy of PVC vary considerably, possibly due to the different temperature programs used and the type of PVC sample studied. For example, Sanchez-Jimenez et al. [30] have reported an E_α of 114 kJ/mol for HCl-PVC whereas Miranda et al. [31] have obtained 198 kJ/mol. However, the trend in activation energies for the three pseudo-components agrees with those generally found in literature : $E_{\alpha,\,P1} < E_{\alpha,\,HCl} < E_{\alpha,\,P2}$ [31–33]. Furthermore, the co-pyrolysis pseudo-components, H-HCl and C-HCl, have average E_α values of 97.9 and 101.7 kJ/mol respectively which are lower than those obtained for their pure-sample counterparts. This observed catalytic effect of HCl on

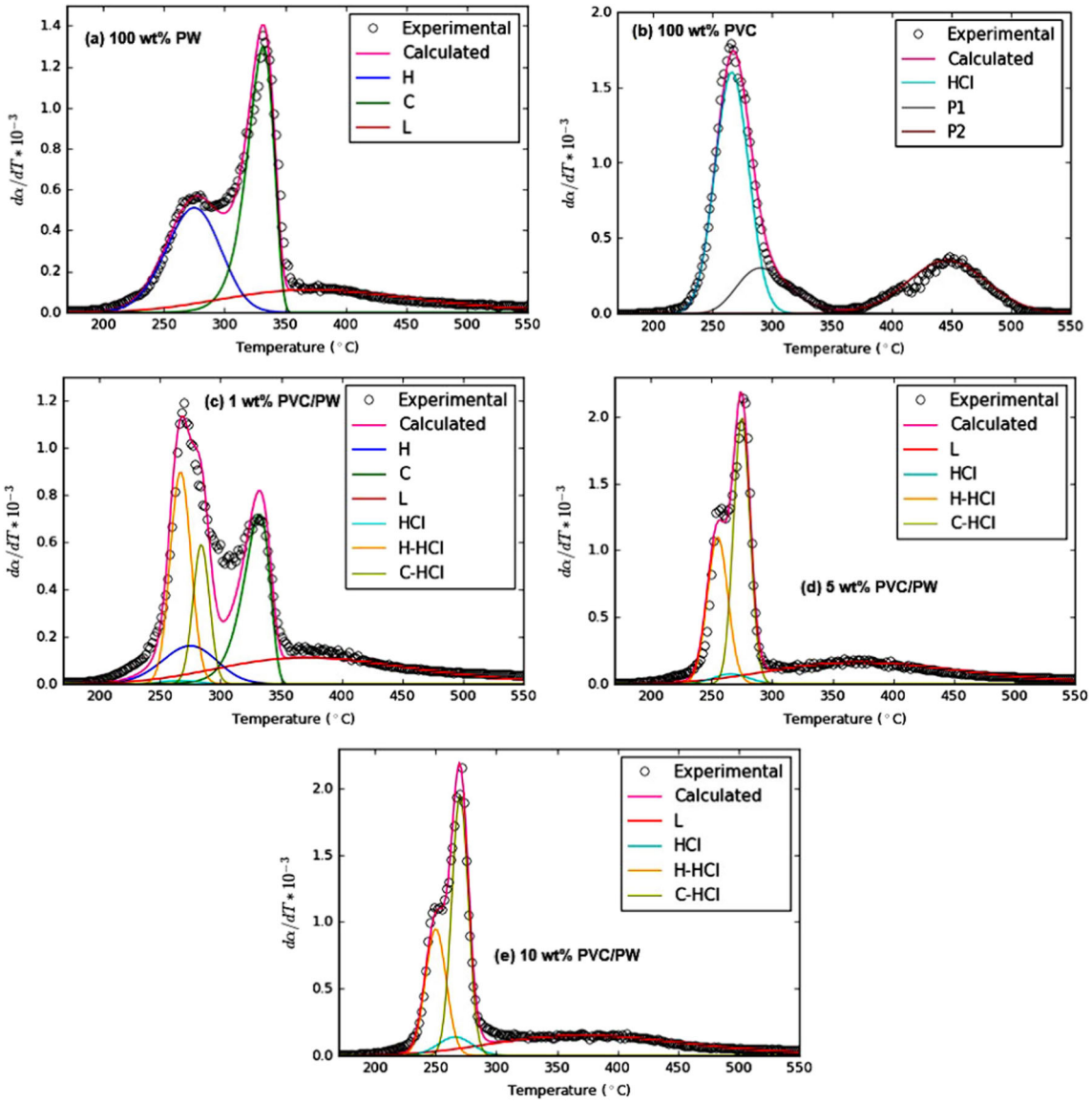

Fig. 3 Deconvoluted DTG curves of pellets of **a** poplar wood (PW), **b** PVC, **c** 1 wt% PVC/PW, **d** 5 wt% PVC/PW, and **e** 10 wt% PVC/PW at 5 °C/min

cellulosic fibres is supported by the experimental work of Matsuzawa et al. [13] who have shown that HCl evolution from PVC catalyses the dehydration and charring of cellulose to form H_2O, CO, CO_2, char and other volatiles. In addition, new findings show that the depolymerisation of cellulose to produce levoglucosan during pyrolysis can be catalysed by H_2O or neighbouring OH^- groups [17, 34, 35]. Hence, HCl can also indirectly catalyse cellulose depolymerisation via the formation of more H_2O from the dehydration process.

5.3 Master plots for kinetic model determination

Figure 6 shows the theoretical master plots of the kinetic models listed in Table 2, as well as the master plots of experimental data corresponding to each pseudo-component. Based on these master plots, the following suitable models have been identified.

Order-based (F) models best describe pseudo hemicellulose (H), lignin (L), $P1$ and $P2$ pyrolysis. An order-based model with a reaction order other than $n = 0$, 1, 2 and 3, is semi-empirical in solid-state kinetics, and hence, it may be a combined effect of other mechanisms such as nucleation and diffusion as is the case for hemicellulose pyrolysis [20, 36]. A reaction order of $n = 1.4$ was obtained for hemicellulose decomposition which is identical to the recently published result by Wang et al. [20] and also falls within the range, $n = 1 - 2$, reported in literature [19, 37, 38]. As for pseudo-lignin, a high reaction order between $n = 4$ and $n = 5$ was reached when matched with the experimental results. This behaviour of lignin may be linked to its highly complex phenylpropane composition whose degradation may involve several mechanisms

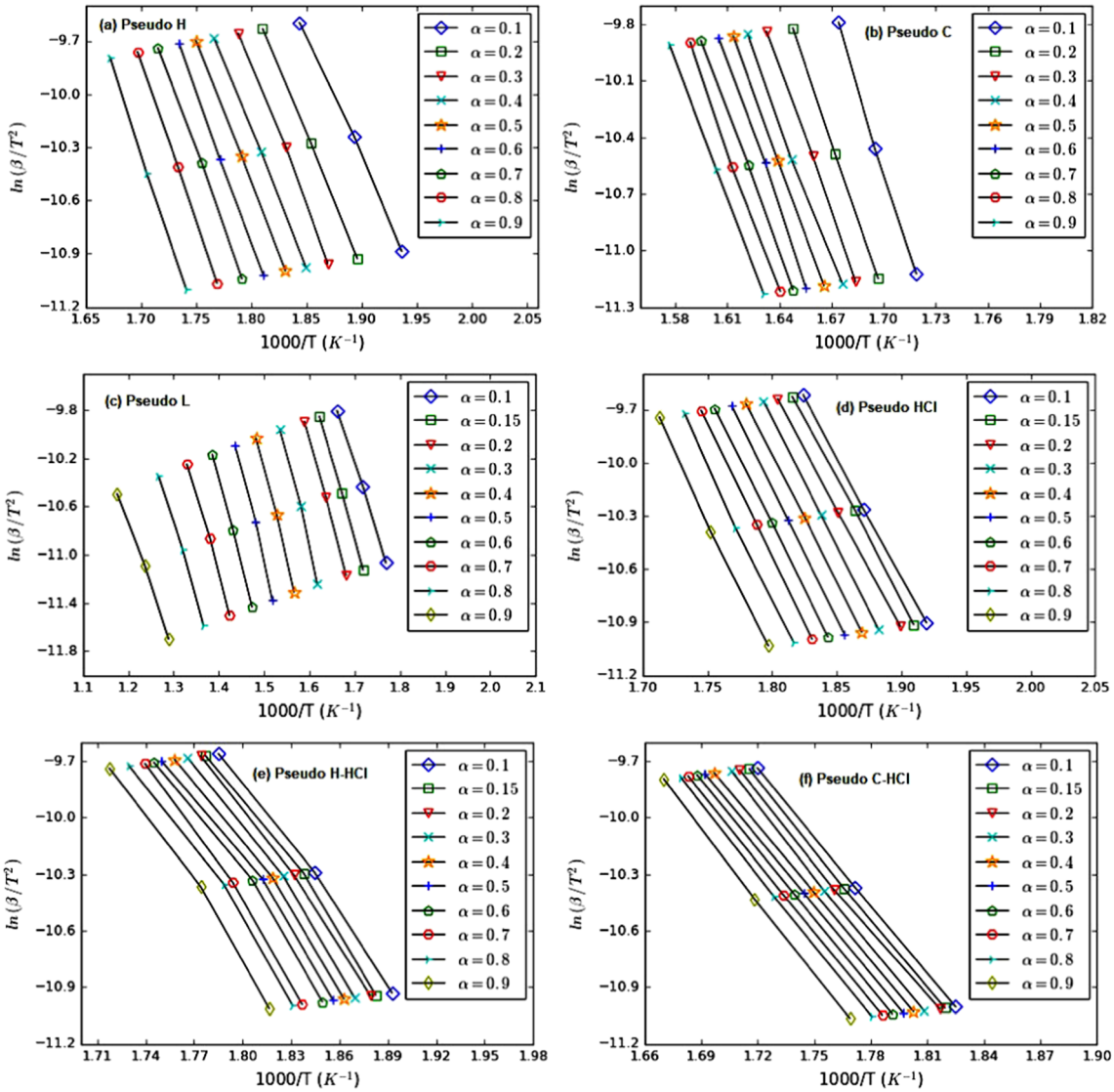

Fig. 4 KAS plots for the pseudo-components between conversions of 0.1 and 0.9

occuring simultaneously. Furthermore, for *P*1 and *P*2, reaction orders of $n = 1$ and $n = 2.5$ can be observed. Solid-state kinetic mechanisms for these two pseudo-components have not yet been found in literature in order to compare with our results.

The Random scission (L2) function most adequately models cellulose (*C*) and HCl degradation. Random scission is an "acceleratory" type model which assumes that bond breaking occurs randomly along the polymer chains, producing fragments of progressively shorter length that eventually evaporate when they are small enough [18, 39]. This mechanism for cellulose pyrolysis has recently been reported by several authors [15–17, 40] and can be associated with intra-ring scission of the glucose unit in the cellulose chain during dehydration and charring reactions [13]. Regarding pseudo HCl-PVC decomposition via dehydrochlorination, the observed random scission mechanism may stem from β-scission reactions that occur along the polymer chain leading to the reduction in chain length and the formation of polyene molecules [27].

Avrami-Erofeev (A) equations best model H − HCl and C − HCl pseudo-components. An Avrami-Erofeev model is also an "acceleratory" type model and is based on nucleation and growth of crystals formed from chemical reactions [28, 41]. Both pseudo H − HCl and C − HCl have an n value of 2, representing two-dimensional growth of crystal nuclei, assuming that the number of nuclei remains constant. This A2 reaction mechanism for H − HCl and C − HCl decomposition signals a rate-limiting acid-base reaction between HCl and minerals in wood (Table 1) to form metal chloride salt crystals (e.g. $CaCl_2$, NaCl and KCl).

A summary of the kinetic model results for PW, PVC and PVC/PW pyrolysis is presented in Table 5 and Table 6.

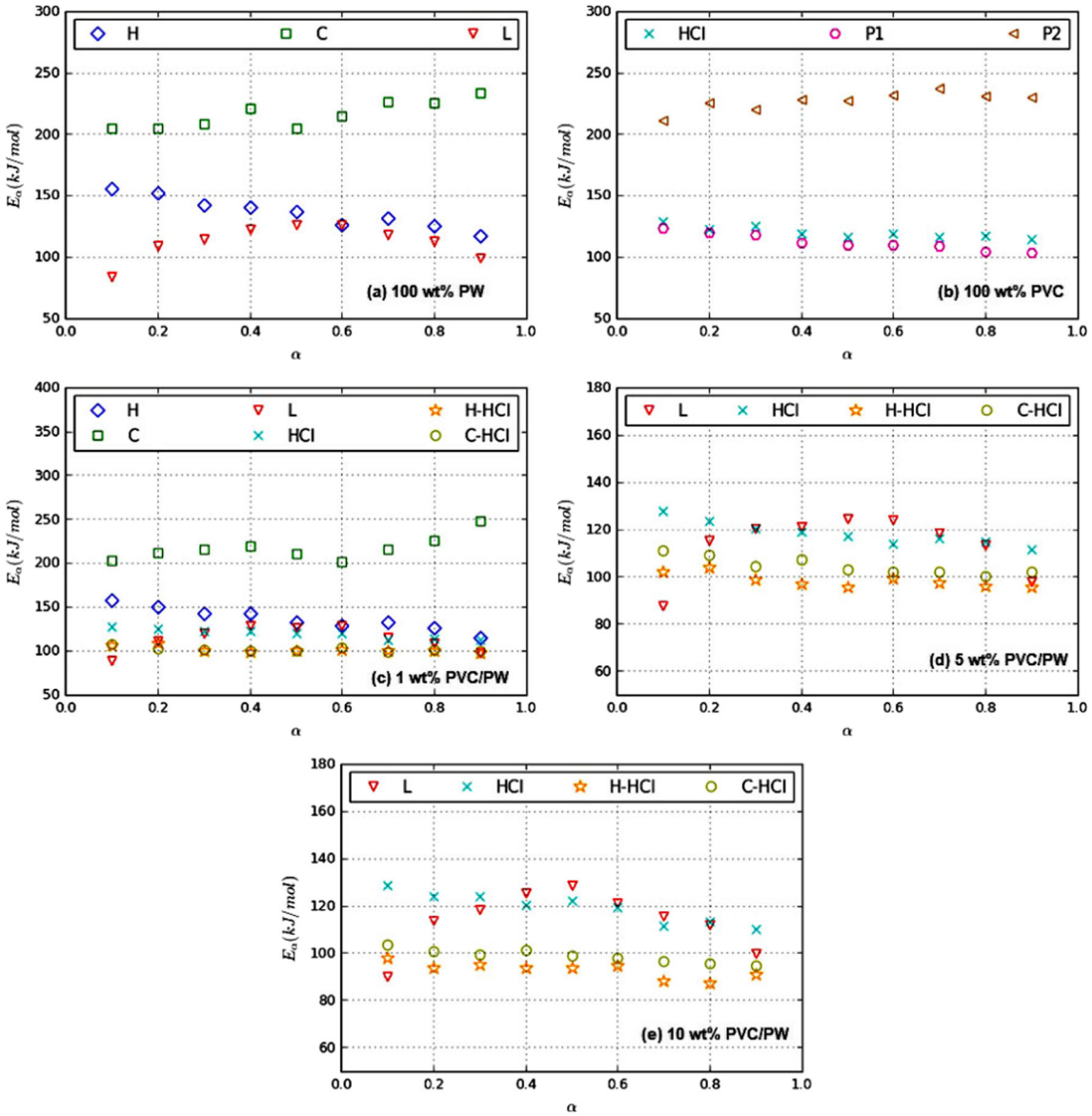

Fig. 5 Activation energy distribution as a function of conversion of the pseudo-components in **a** poplar wood (PW), **b** PVC, **c** 1 wt% PVC/PW, **d** 5 wt% PVC/PW, and **e** 10 wt% PVC/PW

With regard to pseudo-lignin (L), a new kinetic model, F3*: $f(\alpha) = (1-\alpha)^{2.9577}\alpha^{-0.008}$, was determined using the nonlinear least squares regression and the Evolutionary Solver in Excel to fit the experimental data via minimising the deviation parameter in Eq. 20. The optimal pre-exponential factors A were also determined using this method. It can be seen in Table 5 and Table 6 that the deviation between the predicted DTG data and the experimental ones is less than 4.5% for all samples, which is considered to be a good agreement.

6 Conclusion

The work presented in this paper deals with the development and validation of a multi-step kinetic model that predicts the pyrolysis behaviour and reaction mechanism of poplar wood pellets with different contents of PVC. Thermogravimetric experiments at different heating rates were conducted, and apparent kinetic parameters were determined by combining Fraser-Suzuki deconvolution, isoconversional ("model-free") methods and master plot procedures. Our model fits the experimental data well with a deviation of less than 4.5%.

The model results show that at a low PVC concentration of 1 wt%, the apparent activation energies of the pseudo-components of PW, hemicellulose and cellulose, decrease from 136.3 to 101.6 kJ/mol and from 216.7 to 108.2 kJ/mol, respectively. Moreover, increasing the concentration of PVC by a factor of 5 and 10 further decreases the activation energy of hemicellulose by 2.8 kJ/mol and 8.3 kJ/mol and that of cellulose by 3.6 and 9.5 kJ/mol, respectively. The observed

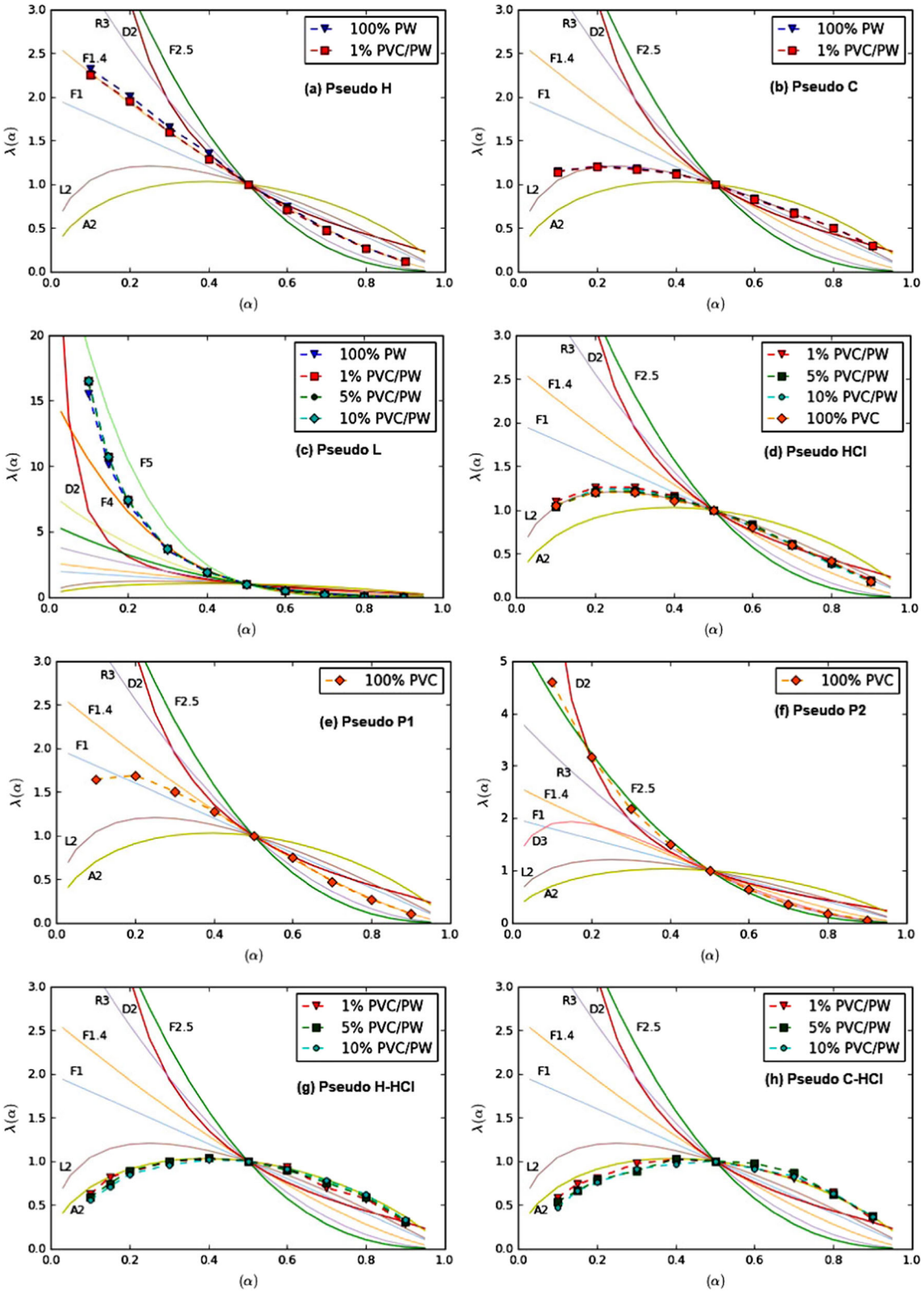

Fig. 6 Comparisons between experimental and theoretical mechanistic models according to the generalised master plot procedure

decrease in activation energies is due to acid hydrolysis of the cellulosic fibres by HCl which is formed from the dehydrochlorination of PVC during pyrolysis.

The reaction mechanism or rate-limiting step for the interaction between PVC and PW was identified to be a nucleation and growth mechanism that follows the

Table 5 Kinetic parameters for the pyrolysis of pure PW and PVC pellets. Values have been averaged over heating rates of 5, 10 and 20 °C/min

Component		100 wt% PW	100 wt% PVC
H	E (kJ/mol)	136.2	-
	A (min^{-1})	7.7×10^{13}	-
	Model	F1.4	-
	c	0.37	-
C	E (kJ/mol)	215.9	-
	A (min^{-1})	8.3×10^{19}	-
	Model	L2	-
	c	0.42	-
L	E (kJ/mol)	110.7	-
	A (min^{-1})	2.7×10^{9}	-
	Model	F3*	-
	c	0.24	-
HCl	E (kJ/mol)	-	119.7
	A (min^{-1})	-	7.5×10^{12}
	Model	-	L2
	c	-	0.56
P1	E (kJ/mol)	-	112.2
	A (min^{-1})	-	6.8×10^{10}
	Model	-	F1
	c	-	0.23
P2	E (kJ/mol)	-	225.9
	A (min^{-1})	-	2.5×10^{17}
	Model	-	F2.5
	c	-	0.21
Dev (%)		4.1	3.2

F3*: $f(\alpha) = (1-\alpha)^{2.9577}\,\alpha^{-0.008}$

Avrami-Erofeev model with $n = 2$ ($A2$). This kinetic model has been linked to the formation and growth of metal chloride crystals as a result of acid-base reactions between HCl and minerals in PW.

Table 6 Kinetic parameters for the pyrolysis of PVC/PW pellets. Values have been averaged over heating rates of 5, 10 and 20 °C/min

Component		1 wt% PVC/PW	5 wt% PVC/PW	10 wt% PVC/PW
H	E (kJ/mol)	136.3	-	-
	A (min^{-1})	2.6×10^{13}	-	-
	Model	F1.4	-	-
	c	0.12	-	-
C	E (kJ/mol)	216.7	-	-
	A (min^{-1})	5.6×10^{19}	-	-
	Model	L2	-	-
	c	0.25	-	-
L	E (kJ/mol)	112.6	112.2	112.6
	A (min^{-1})	3.6×10^{9}	5.4×10^{9}	5.5×10^{9}
	Model	F3*	F3*	F3*
	c	0.21	0.29	0.29
HCl	E (kJ/mol)	120.1	119	119.9
	A (min^{-1})	6.4×10^{10}	3.2×10^{11}	7.5×10^{11}
	Model	L2	L2	L2
	c	0.0053	0.0301	0.0583
H-HCl	E (kJ/mol)	101.6	98.8	93.3
	A (min^{-1})	3.8×10^{10}	4.1×10^{10}	1.3×10^{10}
	Model	A2	A2	A2
	c	0.25	0.27	0.25
C-HCl	E (kJ/mol)	108.2	104.6	98.7
	A (min^{-1})	1.4×10^{10}	1.2×10^{11}	3.8×10^{10}
	Model	A2	A2	A2
	c	0.16	0.41	0.41
Dev (%)		4.5	1.9	2.0

F3*: $f(\alpha) = (1-\alpha)^{2.9577}\,\alpha^{-0.008}$

To date, the few kinetic models reported in the literature on the co-pyrolysis of biomass and PVC assumed a single-step co-pyrolysis model and/or first-order reaction mechanism. These assumptions have been shown by several authors to often give inaccurate kinetic parameters. Thus, this work represents a step forward on the determination of kinetic models for co-pyrolysis of biomass and PVC. Furthermore, a key advantage of our model is its relative simplicity, which makes it readily usable in a reactor-scale model of a pyro-gasifier. This latter is crucial for the valorisation of wood waste into valuable products including biomass-derived hydrogen.

Future work will report the exploitation of this model for the pyrolysis/gasification of wood waste at large pilot scale.

Acknowledgments The authors gratefully thank our colleagues at RAPSODEE research centre for technical help.

Funding information The study was financially supported by Suez Environnement (France) and IMT Mines Albi.

References

1. JRC-IPTS (2010) Study on the selection of waste streams for end-of-waste assessment. JRC Scientific and Technical Reports, EUR 24362, https://ec.europa.eu/jrc/en/publication/eur-scientific-and-technical-research-reports/study-selection-waste-streams-end-waste-assessment-final-report (Accessed August 1st, 2020).
2. Fail S, Diaz N, Benedikt F, Kraussler M, Hinteregger J, Bosch K, Hackel M, Rauch R, Hofbauer H (2014) Wood gas processing to generate pure hydrogen suitable for PEM fuel cells. ACS Sustain Chem Eng 2(12):2690–2698. https://doi.org/10.1021/sc500436m
3. Pal DB, Chand R, Upadhyay SN, Mishra PK (2018) Performance of water gas shift reaction catalysts: a review. Renew Sust Energ Rev 93:549–565. https://doi.org/10.1016/j.rser.2018.05.003
4. Grande CA (2016) PSA Technology for H_2 Separation. In: Stolten D, Emonts B (eds) Hydrogen science and engineering: materials, processes, systems and technology. Wiley-VCH Verlag GmbH & Co. KGaA, Boschstr. 12, 69469 Weinheim, Germany.
5. Hale SE, Lehmann J, Rutherford D, Zimmerman AR, Bachmann RT, Shitumbanuma V, O'Toole A, Sundqvist KL, Arp HPH, Cornelissen G (2012) Quantifying the total and bioavailable polycyclic aromatic hydrocarbons and dioxins in biochars. Environ Sci Technol 46:2830–2838
6. Zhou H, Long Y, Meng A, Li Q, Zhang Y (2015) Interactions of three municipal solid waste components during co-pyrolysis. J Anal Appl Pyrolysis 111:265–271. https://doi.org/10.1016/j.jaap.2014.08.017
7. Yu J, Sun L, Ma C, Qiao Y, Yao H (2016) Thermal degradation of PVC: a review. Waste Manag 48:300–314. https://doi.org/10.1016/j.wasman.2015.11.041
8. Han B, Chen Y, Wu Y, Hua D, Chen Z, Feng W, Yang M, Xie Q (2014) Co-pyrolysis behaviors and kinetics of plastics-biomass blends through thermogravimetric analysis. J Therm Anal Calorim 115(1):227–235. https://doi.org/10.1007/s10973-013-3228-7
9. Çepelioğullara Ö, Pütün AE (2013) Thermal and kinetic behaviors of biomass and plastic wastes in co-pyrolysis. Energy Convers Manag 75:263–270. https://doi.org/10.1016/j.enconman.2013.06.036
10. Miskolczi N, Bartha L, Angyal A (2009) Pyrolysis of polyvinyl chloride (PVC)-containing mixed plastic wastes for recovery of hydrocarbons. Energy Fuel 23:2743–2749. https://doi.org/10.1021/ef8011245
11. Bai XY, Wang QW, Sui SJ, Zhang CS (2011) The effects of wood-flour on combustion and thermal degradation behaviors of PVC in wood-flour/poly(vinyl chloride) composites. J Therm Anal Calorim 91(1):34–39. https://doi.org/10.1016/j.jaap.2011.02.009
12. Sorum L, Gronli M, Hustad J (2000) Pyrolysis characteristics and kinetics of municipal solid wastes. Fuel 80(9):1217–1227. https://doi.org/10.1016/S0016-2361(00)00218-0
13. Matsuzawa Y, Ayabe M, Nishino J (2001) Acceleration of cellulose co-pyrolysis with polymer. Polym Degrad Stab 71(3):435–444. https://doi.org/10.1016/S0141-3910(00)00195-6
14. Sanchez-Jimnez PE, Prez-Maqueda LA, Perejn A, Criado JM (2013) Generalized master plots as a straightforward approach for determining the kinetic model: the case of cellulose pyrolysis. Thermochim Acta 552:54–59. https://doi.org/10.1016/j.tca.2012.11.003
15. Aboulkas A, El Harfi K (2009) Co-pyrolysis of olive residue with poly (vinyl chloride) using thermogravimetric analysis. J Thermal Anal Calorim 95(3):1007–1013. https://doi.org/10.1007/s10973-008-9315-5
16. Vyazovkin S, Burnham AK, Criado JM, Prez-Maqueda LA, Popescu C, Sbirrazzuoli N (2011) ICTAC Kinetics Committee recommendations for performing kinetic computations on thermal analysis data. Thermochim Acta 520(1-2):1–19. https://doi.org/10.1016/j.tca.2011.03.034
17. Burnham AK, Zhou X, Broadbelt LJ (2015) Critical review of the global chemical kinetics of cellulose thermal decomposition. Energy Fuel 29(5):2906–2918. https://doi.org/10.1021/acs.energyfuels.5b00350
18. Sanchez-Jimnez PE, Prez-Maqueda LA, Perejn A, Criado JM (2010) Generalized kinetic master plots for the thermal degradation of polymers following a random scission mechanism. J Phys Chem A 114(30):7868–7876. https://doi.org/10.1021/jp103171h
19. Hu S, Jess A, Xu M (2007) Kinetic study of Chinese biomass slow pyrolysis: comparison of different kinetic models. Fuel 86(17-18):2778–2788. https://doi.org/10.1016/j.fuel.2007.02.031
20. Wang X, Hu M, Hu W, Chen Z, Liu S, Hu Z, Xiao B (2016) Thermogravimetric kinetic study of agricultural residue biomass pyrolysis based on combined kinetics. Bioresour Technol 219:510–520. https://doi.org/10.1016/j.biortech.2016.07.136
21. Cagnon B, Py X, Guillot A, Stoeckli F, Chambat G (2009) Contributions of hemicellulose, cellulose and lignin to the mass and the porous properties of chars and steam activated carbons from various lignocellulosic precursors. Bioresour Technol 100:292–298. https://doi.org/10.1016/j.biortech.2008.06.009
22. Zhou J, Gui B, Qiao Y, Zhang J, Wang W, Yao H, Yu Y, Xu M (2016) Understanding the pyrolysis mechanism of polyvinylchloride (PVC) by characterizing the chars produced in a wire-mesh reactor. Fuel 166:526–532. https://doi.org/10.1016/j.fuel.2015.11.034
23. Mehl M, Marongiu A, Faravelli T, Bozzano G, Dente M, Ranzi E (2004) A kinetic modeling study of the thermal degradation of halogenated polymers. J Anal Appl Pyrolysis 72(2):253–272. https://doi.org/10.1016/j.jaap.2004.07.007
24. Slopiecka K, Bartocci P, Fantozzi F (2012) Thermogravimetric analysis and kinetic study of poplar wood pyrolysis. Appl Energy 97:491–497. https://doi.org/10.1016/j.apenergy.2011.12.056
25. Hu M, Chen Z, Wang S, Guo D, Ma C, Zhou Y, Chen J, Laghari M, Fazal S, Xiao B, Zhang B, Ma S (2016) Thermogravimetric kinetics of lignocellulosic biomass slow pyrolysis using distributed activation energy model, Fraser-Suzuki deconvolution, and iso-conversional method. Energy Convers Manag 118:1–11. https://doi.org/10.1016/j.enconman.2016.03.058

26. Davis PJ, Rabinowitz P (2007) Methods of numerical integration, 2nd edn. Dover Publications, Inc., Meneola, New York
27. Marongiu A, Faravelli T, Bozzano G, Dente M, Ranzi E (2003) Thermal degradation of poly(vinyl chloride). J Anal Appl Pyrolysis 70(2):519–553. https://doi.org/10.1016/S0165-2370(03)00024-X
28. De Bruijn TJW, De Jong WA, Van Den Berg PJ (1981) Kinetic parameters in Avrami-Erofeev type reactions from isothermal and non-isothermal experiments. Thermochim Acta 45(3):315–325. https://doi.org/10.1016/0040-6031(81)85091-5
29. Anca-Couce A (2016) Reaction mechanisms and multi-scale modelling of lignocellulosic biomass pyrolysis. Prog Energy Combust Sci 53:41–79. https://doi.org/10.1016/j.pecs.2015.10.002
30. Sanchez-Jimnez PE, Perejn A, Criado JM, Dinez MJ, Prez-Maqueda LA (2010) Kinetic model for thermal dehydrochlorination of poly(vinyl chloride). Polymer 51(17):3998–4007. https://doi.org/10.1016/j.polymer.2010.06.020
31. Miranda R, Yang J, Roy C, Vasile C (1999) Vacuum pyrolysis of PVC I. Kinetic study. Polym Degrad Stab 64(1):127–144. https://doi.org/10.1016/S0141-3910(98)00186-4
32. Bhargava A, van Hees P, Andersson B (2016) Pyrolysis modeling of PVC and PMMA using a distributed reactivity model. Polym Degrad Stab 129:199–211. https://doi.org/10.1016/j.polymdegradstab.2016.04.016
33. Miranda R, Yang J, Roy C, Vasile C (2001) Vacuum pyrolysis of commingled plastics containing PVC I. Kinetic study. Polym Degrad Stab 72(3):469–491. https://doi.org/10.1016/S0141-3910(01)00048-9
34. Seshadri V, Westmoreland PR (2014) Role of pericyclic reactions in the pyrolysis of cellulose and hemicellulose. In: Role of pericyclic reactions in the pyrolysis of cellulose and hemicellulose, San Francisco, CA, vol Paper ENFL-133.
35. Seshadri V, Westmoreland PR (2012) Concerted reactions and mechanism of glucose pyrolysis and implications for cellulose kinetics. J Phys Chem A 116(49):11,997–12,013. https://doi.org/10.1021/jp3085099
36. Bar-Gadda R (1980) The kinetics of xylan pyrolysis. Thermochim Acta 42(2):153–163. https://doi.org/10.1016/0040-6031(80)87099-7
37. Tran KQ, Bach QV, Trinh TT, Seisenbaeva G (2014) Non-isothermal pyrolysis of torrefied stump – a comparative kinetic evaluation. Appl Energy 136:759–766. https://doi.org/10.1016/j.apenergy.2014.08.026
38. Li Z, Zhao W, Meng B, Liu C, Zhu Q, Zhao G (2008) Kinetic study of corn straw pyrolysis: comparison of two different three-pseudocomponent models. Bioresour Technol 99(16):7616–7622. https://doi.org/10.1016/j.biortech.2008.02.003
39. Staggs JEJ (2002) Modelling random scission of linear polymers. Polym Degrad Stab 76(1):37–44. https://doi.org/10.1016/S0141-3910(01)00263-4
40. Samuelsson LN, Moriana R, Babler MU, Ek M, Engvall K (2015) Model-free rate expression for thermal decomposition processes: the case of microcrystalline cellulose pyrolysis. Fuel 143:438–447. https://doi.org/10.1016/j.fuel.2014.11.079
41. Brown ME (1998) Handbook of thermal analysis and calorimetry: Principles and practice, vol 1. Elsevier, Amsterdam